Pion quasiparticles in isospin medium from holography

Weijian Liang, Xuanmin Cao,* Hui Liu, and Danning Li†
Department of Physics and Siyuan Laboratory, Jinan University, Guangzhou 510632, China

(Received 23 July 2023; accepted 31 October 2023; published 21 November 2023)

The properties of the pion quasiparticle in hot and dense isospin medium, including the screening mass, pole mass, and thermal width, as well as their relationships with the pion superfluid phase transition, are investigated in the framework of two-flavor ($N_f = 2$) soft-wall AdS/QCD models. We extract the screening mass of the pion from the pole of the spatial two-point retarded correlation function. The screening masses of both neutral and charged pions increase monotonously with the increasing of temperature. However, the isospin chemical potential μ_I would depress the screening masses of the charged pions, $m_{\pi^\pm,\mathrm{scr}}$. With the increasing of μ_I, $m_{\pi^\pm,\mathrm{scr}}$ monotonically decrease to zero on the boundary between the normal phase and the pion superfluid phase, while the screening mass of the neutral pion, $m_{\pi^0,\mathrm{scr}}$, remains almost unchanged. We also extracted the pole mass m_{pole} and thermal width Γ of the pion from the pole of temporal two-point retarded correlation function, i.e., the corresponding quasinormal frequencies, $\omega = m_{\mathrm{pole}} - i\Gamma/2$. The pole masses of the three modes (π^0, π^+, π^-) are splitting at finite μ_I. The thermal widths of the three modes increase with temperature. Furthermore, the pole mass and thermal width of π^+ decrease almost monotonically with the increasing of μ_I, reaching zero at $\mu_I = \mu_I^c$, simultaneously. It indicates that π^+ becomes a massless Goldstone boson as a result of the pion superfluid phase transition.

DOI: 10.1103/PhysRevD.108.096019

I. INTRODUCTION

The fundamental theory of the strong interaction is quantum chromodynamics (QCD) and the strongly interacting matter possesses rich phase structure in the condition of finite temperature and density. By creating the circumstance of high temperature and high density from the Relativistic Heavy Ion Collision (RHIC) experiments, one can investigate the QCD phase transitions which are not only important to realize the QCD phase structure, but also are critical to understand the evolution of the early Universe and the internal structure of quark stars [1–4]. At low temperature and density, the strongly interacting matter is in the hadronic phase. The transition from hadronic phase to quark-gluon plasma (QGP) phase, namely the deconfinement transition, takes place with the increasing of temperature and chemical potential. Besides, the transition from the chiral symmetry breaking phase to the chiral symmetry restoration phase occurs with the rise of temperature and chemical potential.

Since the created fireballs in RHICs last for very short time, the detection of the properties of the hot and dense medium is mainly based on the detection of the final particles, among which the hadrons play important roles. In order to make a good explanation to the experimental data from RHICs, it is essential to study the in-medium properties of hadrons which might have significant impacts on their final distribution [5]. Furthermore, understanding the properties of hadrons under the extreme conditions is of scientific merit to reveal the phase structure of strong interaction.

One of the most important quantities to characterize the properties of meson is the meson mass, the thermal and dense behaviors of which are of significance to understand the properties of hot and dense nuclear matter. Due to the breaking of the Lorentz symmetry at finite temperature, one can define two different kinds of meson mass in medium, namely, screening mass and pole mass.

Defined as the exponential decay of the spatial correlator, the screening mass encodes the information of spatial correlation function of meson field. Quantitatively, the screening mass is defined by the pole of spatial correlation function in momentum space, i.e., $G^{-1}(\boldsymbol{p})|_{\boldsymbol{p}^2=-m_{\mathrm{scr}}^2} = 0$ [6–8]. Physically, the inverse of screening mass, a characteristic spatial distance, can describe the screening effect that a test hadron put inside the hot medium can be effectively screened beyond this spatial distance [8].

The pole mass is defined by the real part of the pole of the temporal correlator $G(\omega)$ in the frequency space. Physically, the pole mass depicts the natural oscillation

*Corresponding author: caoxm@jnu.edu.cn
†Corresponding author: lidanning@jnu.edu.cn

frequency of a particle. At $T = 0$, the screening mass is equal to the pole mass because of the Lorentz invariance of the system. However, the screening mass and the pole mass are different at $T > 0$ because the Lorentz invariance is broken by the existence of a heat bath reference frame [9–11].

Apart from the masses mentioned above, the thermal width, which is defined by the imaginary part of the pole of the temporal correlator $G(\omega)$ and interpreted as resonance absorption in hot and dense nuclear matter, is also an important quantity to characterize the properties of meson in-medium. The thermal width of meson has an important effect in RHICs. For example, the temperature dependence of the thermal width of the ρ meson is of significance to measure the dilepton production in the heavy ion collision [12]. Besides, a monotonically increasing mesonic width with increasing T can be related to a signal of deconfinement transition [13,14].

Among the light mesons, of particular interest is the pion, known as the lightest meson as well as pseudo-Goldstone boson, which has attracted many attentions in recent years. There are several reasons to investigate the in-medium properties of pion. First, it is the lightest meson so that it can reach thermal equilibrium with the medium easily. Furthermore, pion has a close relationship with chiral phase transition. For example, in chiral limit, the mass of pion vanishes but that of scalar meson does not below the chiral phase transition temperature T_c. However, above T_c, the mass of pion becomes finite and gets degenerate with scalar meson as temperature rises, which indicates the transition from the chiral symmetry breaking phase to the chiral symmetry restoration phase. What is more, at hadronic spectrum level, pion in isospin medium is also a probe for pion superfluid phase transition. When the isospin chemical potential μ_I grows to m_π at zero temperature, the U(1) symmetry is broken spontaneously and the pion superfluid phase occurs [15]. The study of the isospin behavior of pion remains an interesting topic in hadronic physics. On the one hand, the isospin density effect can be verified directly by the lattice simulation without serious technical problems [16,17]. On the other hand, the Goldstone mode corresponding to the global isospin symmetry breaking plays a leading role on the dynamic and thermal properties of the pion superfluidity [18].

The physics of the pion at finite temperature and isospin density, however, is nonperturbative. Thus, the development of nonperturbative methods is necessary. Lattice QCD (LQCD) simulation [6,19,20], as a first-principle calculation, can work very well at finite temperature. But LQCD is complicated at finite chemical potential due to the sign problem of the fermion determinant [21]. Other low energy effective models are constructed to describe the properties of pion, such as the chiral perturbation theory (χPT) [22,23], the functional renormalization group (FRG) [24,25], the Dyson-Schwinger equation (DSE) [26,27] and the Nambu-Jona-Lasinio model (NJL) [28–35]. Different methods lead to the same conclusion that the pion masses increase with the increasing of temperature above the chiral transition temperature T_c. However, the temperature behavior of the pion pole mass with physical quark mass below T_c is still controversial now. Son and Stephanov argue that $m_{\pi,\text{pole}}$ decreases with the increasing of temperature below T_c [22,23]. This argument is supported by the LQCD [19,20] and the NJL model with gluon condensation [28]. However, other methods including FRG [24], NJL models [31], LQCD [6], and DSEs [27] obtain an opposite result that $m_{\text{pole},\pi}$ increases with the increasing of temperature below T_c. Therefore, it is necessary to use other methods to study this problem.

Developed from the anti-de Sitter/conformal field theory (AdS/CFT) correspondence [36–38], fortunately, holographic method provide an alternative robust approach to deal with the strong coupling problem of QCD [39]. There are lots of useful models in the framework of bottom-up approach, such as the hard-wall model [40], the soft-wall model [41], the light-front holographic QCD [42] and the Einstein-Maxwell-Dilaton model [43–47]. Among these models, the soft-wall AdS/QCD model and its extended models give a good description of the chiral phase transition [48–59]. These models can also describe the glueball and hadron spectra well [60–73]. Consequently, we would like to investigate the pion spectra in the framework of soft-wall AdS/QCD model.

There are many efforts have been made to investigate the isospin behavior of pion in the hard-wall model [74–78] and the soft-wall model [79,80]. However, most of these literatures consider temperature and isospin density effect separately. It is meaningful to consider both of them at the same time and study the mutual effects for the pion spectra. Based on the soft-wall AdS/QCD model, there are some investigations on the pion pole mass, screening mass and their thermal properties at finite temperature and isospin chemical potential [67,68] through the spectral function method.[1] As temperature rises, however, the resonance peak of the spectrum function gets inconspicuous and it is difficult to determine its location. Therefore, in this paper, we resort to another method by calculating the quasi-normal frequency of the quasi-normal mode(QNM), the real and imaginary part of which denote the pole mass and the thermal width, respectively [86,87]. Through the QNM method, we extend the study [68] to finite μ_I to investigate the isospin behavior of screening mass as well as the relationship between the pion spectra and the pion superfluid phase transition.

[1]The spectral function method has been widely used in the studies in holographic QCD models [81–84]. Furthermore, the spectral function can also extracted from the lattice data from the spatial correlator [85].

The paper is organized as follows. In Sec. II, we will give a brief review of the soft-wall AdS/QCD model. In Sec. III, we will extract the screening masses of pion quasiparticles by calculating the poles of the spatial correlation functions at finite temperature and isospin chemical potential. We will also study the temporal correlation functions and extract the pole masses and thermal widths from QNMs. In Sec. IV we will give our conclusion and summary.

II. SOFT-WALL AdS/QCD MODELS WITH FINITE ISOSPIN CHEMICAL POTENTIAL

In the bottom-up approach, the soft-wall AdS/QCD model [41] can describe both spontaneously chiral symmetry breaking and linear confinement in the vacuum qualitatively. Here, we review the soft-wall AdS/QCD model briefly.

The action of $N_f = 2$ soft-wall AdS/QCD model constructed with the $\mathrm{SU}(2)_L \times \mathrm{SU}(2)_R$ gauge symmetry under the dual 5D geometry [41] takes the following form

$$S = \int d^4x \int dz \sqrt{g} e^{-\Phi} \mathrm{Tr}\Big\{ |D_M X|^2 - V(|X|) - \frac{1}{4g_5^2}(F_L^2 + F_R^2) \Big\}, \tag{1}$$

where g is the determinant of the metric g_{MN}. $\Phi(z) = \mu_g^2 z^2$ is the quadratic dilaton field which depends on the fifth dimension z [41]. When the number of colors is $N_c = 3$, the gauge coupling constant g_5 equals 2π by comparing the vector current two-point function in large-momentum expansion to the large-N_c QCD perturbative result [40]. We will take $N_c = 3$ in the following calculation. X is the matrix-valued bulk scalar field, and the covariant derivative $D_M X$ with $M = (x, z)$ is defined as

$$D_M X = \partial_M X - i L_M X + i X R_M, \tag{2}$$

where L_M and R_M are the chiral gauge fields,

$$L_M = L_M^a t^a, \qquad R_M = R_M^a t^a. \tag{3}$$

$t^a = \sigma^a/2$ $(a = 1, 2, 3)$ are the generators of SU(2). The potential term takes

$$V(|X|) = m_5^2 |X|^2 + \lambda |X|^4, \tag{4}$$

with the modified 5D mass $m_5^2(z)$ [55] and a free parameter λ. $F_{MN}^{L/R}$ are the field strength tensors of the corresponding chiral gauge fields, which are defined by

$$F_{MN}^L = \partial_M L_N - \partial_N L_M - i[L_M, L_N], \tag{5a}$$

$$F_{MN}^R = \partial_M R_N - \partial_N R_M - i[R_M, R_N]. \tag{5b}$$

For convenience, we can redefine the chiral gauge fields as the vector gauge field and the axial-vector gauge field

$$V_M = \frac{L_M + R_M}{2}, \tag{6a}$$

$$A_M = \frac{L_M - R_M}{2}, \tag{6b}$$

where the vector field V_M and the axial-vector field A_M are dual to the vector current J_μ^V and axial-vector current J_μ^A, respectively. For example, the isospin current $\bar{q}\gamma_\mu t^3 q$ is dual to V_μ^3. After the transformation in Eq. (6), we obtain the gauge field strengths

$$F_{MN}^V = \partial_M V_N - \partial_N V_M - i[V_M, V_N] - i[A_M, A_N], \tag{7a}$$

$$F_{MN}^A = \partial_M A_N - \partial_N A_M - i[V_M, A_N] - i[A_M, V_N], \tag{7b}$$

and the covariant derivative

$$D_M X = \partial_M X - i[V_M, X] - i\{A_M, X\}. \tag{8}$$

We consider the temperature as well as the isospin chemical potential effect and take the following metric ansatz

$$ds^2 = e^{2A(z)}\left(f(z) dt^2 - d\mathbf{x}^2 - \frac{1}{f(z)} dz^2 \right). \tag{9}$$

If there is a horizon $z = z_h$ where $f(z) = 0$, one can define the temperature by the following formula

$$T = \frac{|f'(z_h)|}{4\pi}. \tag{10}$$

According to the holographic dictionary, the conserved current is dual to the gauge field defined by Eq. (6a). In general, $A(z)$ and $f(z)$ should be solved from a certain kind of gravity system which is coupled with the soft-wall AdS/QCD model action. For simplicity, we calculate in the sense of probe limit. We consider the anti–de Sitter-Reissner-Nordstrom (AdS-RN) metric solution with finite isospin chemical potential

$$A(z) = -\ln(z), \tag{11}$$

$$f(z) = 1 - (1 + \mu_I^2 z_h^2)\frac{z^4}{z_h^4} + \mu_I^2 \frac{z^6}{z_h^4} \tag{12}$$

with the isospin chemical potential μ_I. V_0^3 satisfies the following formula

$$V_0^3(z) = \mu_I \left(1 - \frac{z^2}{z_h^2} \right). \tag{13}$$

For convenience, we denote $V_0^3(z)$ by $\nu(z)$. From Eqs. (10) and (12), we can obtain the temperature as follows

$$T = \frac{2-\mu_I^2 z_h^2}{2\pi z_h}. \tag{14}$$

In this work, we only consider two lightest flavors of quarks, namely up (u) quark and down (d) quark, with the same physical mass $m_u = m_d \equiv m_q$. Then we get the matrix-valued scalar field

$$X = \frac{\chi}{2}\mathrm{I}. \tag{15}$$

Here, I is the two-dimensional identity matrix. Inserting Eqs. (9) and (15) into the 5D action Eq. (1), we can obtain the equation of motion (EOM) of χ as follows

$$\chi'' + \left(3A' - \Phi' + \frac{f'}{f}\right)\chi' - \frac{e^{2A}}{f}\left(m_5^2\chi + \frac{\lambda\chi^3}{2}\right) = 0. \tag{16}$$

By solving the EOM of χ, one can obtain the temperature and isospin chemical potential dependence of chiral condensate. However, it is a second-order nonlinear ordinary differential equation and it is hard to obtain the analytical solution. Therefore, we must resort to the numerical solution.

To obtain general features of the soft-wall AdS/QCD models, herein, we consider two kinds of soft-wall AdS/QCD models with different modified 5D masses $m_5^2(z)$ which are introduced to obtain a good description of both spontaneous chiral symmetry breaking and meson spectrum. The modified forms of $m_5^2(z)$ are shown in Table I. Model I is introduced in Ref. [55]. In model II, we consider the modification of $m_5^2(z)$ as the coupling to the dilaton $\Phi(z)$.

For model I, one can obtain the asymptotic expansion of χ at the UV boundary ($z=0$) and the horizon ($z=z_h$)

$$\chi(z\to 0) = m_q\zeta z + \frac{\sigma}{\zeta}z^3 + \frac{m_q\zeta}{4}(-2\mu_c^2 + 4\mu_g^2 + m_q^2\zeta^2\lambda)z^3\ln(z) + \mathcal{O}(z^4) \tag{17a}$$

$$\chi(z\to z_h) = c_0 + \frac{c_0(2\mu_c^2 z_h^2 - c_0^2\lambda + 6)}{8z_h - 4z_h^3\mu_I^2}(z-z_h) + \mathcal{O}[(z-z_h)^2] \tag{17b}$$

TABLE I. Two kinds of soft-wall AdS/QCD models with different 5D masses $m_5^2(z)$.

Model	I	II
$m_5^2(z)$	$-3-\mu_c^2 z^2$	$-3[1+\gamma\tanh(\kappa\Phi)]$

TABLE II. Parameters in model I [55].

Parameters	m_q (GeV)	μ_g (GeV)	μ_c (GeV)	λ
Value	3.22×10^{-3}	0.44	1.45	80

where the two independent integral constants m_q and σ at the UV boundary are dual to quark mass and chiral condensate $\sigma \equiv \langle\bar{q}q\rangle$, respectively, according to the holographic dictionary. Here, ζ is a normalization constant which equals $\sqrt{N_c}/2\pi$, by matching the correlation of $\bar{q}q$ operator to 4D result [48]. Furthermore, c_0 is a integration constant generating a regular solution at the horizon. For model II, we can also obtain the asymptotic series at the UV boundary ($z=0$) and the horizon ($z=z_h$)

$$\chi(z\to 0) = m_q\zeta z + \frac{\sigma}{\zeta}z^3 + \frac{1}{4}[m_q(4-6\gamma\kappa)\mu_g^2\zeta + m_q^3\lambda\zeta^3]z^3\ln(z) + \mathcal{O}(z^4) \tag{18a}$$

$$\chi(z\to z_h) = c_0 + \frac{c_0[6 - c_0^2\lambda + 6\gamma\tanh(z_h^2\kappa\mu_g^2)]}{8z_h - 4z_h^3\mu_I^2} \times (z-z_h) + \mathcal{O}[(z-z_h)^2] \tag{18b}$$

The parameters of model I, as are shown in Table II, are taken from Ref. [55]. For model II, we adopt the parameters shown in Table III. These parameters can be determined as follows. First, for convenience, we set $\kappa = 1$. Second, following Ref. [88], we fix the parameter μ_g, which is connected to the Regge behavior of the meson spectrum, to $\mu_g = 0.43$ GeV. Third, the parameters λ and m_q are account for the values of pion mass m_π and chiral condensation σ. On the one hand, chiral condensation σ decreases as λ increases. On the other hand, pion mass m_π increases as m_q increases. We aimed to fit m_π to about 139.6 MeV [89] and σ to about 0.0240 GeV^3 [63]. We obtained $\lambda = 14.7$ and $m_q = 3.58$ MeV. Under these fitted parameters, the corresponding values of m_π and σ are about 139.7 MeV and 0.0239 GeV^3, respectively. Finally, the parameter γ is related to the chiral phase transition temperature T_c, which is roughly between 150 and 160 MeV. We obtain $\gamma = 3.7$ and the corresponding transition temperature is about 153 MeV. Furthermore, we can get the pion decay constant $f_\pi \approx \sqrt{2m_q\sigma/m_\pi^2} \approx 0.094$ GeV through the Gell-Mann-Oakes-Renner (GOR) relation with the fitted parameters, which is consistent with the experiment data [89].

TABLE III. Parameters in model II.

Parameters	m_q (GeV)	μ_g (GeV)	γ	λ	κ
Value	3.58×10^{-3}	0.43	3.7	14.7	1

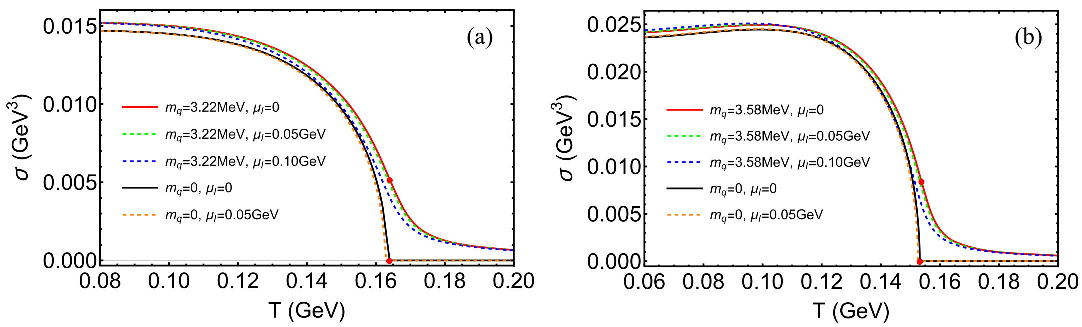

FIG. 1. (a) The chiral condensate σ of model I as a function of temperature T with different isospin chemical potential μ_I in chiral limit ($m_q = 0$) and with physical quark mass ($m_q = 3.22$ MeV), respectively. In chiral limit, σ vanishes at the critical temperature T_c (at $\mu_I = 0$, $T_c \approx 0.1633$ GeV). With finite physical quark mass, however, the second-order phase transition becomes a crossover with the pseudocritical temperature $T_{cp} \approx 0.1639$ GeV at $\mu_I = 0$ (As shown by the red dots). (b) The chiral condensate σ of model II as a function of temperature T with different isospin chemical potential μ_I in chiral limit ($m_q = 0$) and with physical quark mass ($m_q = 3.58$ MeV). The red points in (b) stand for the critical temperature $T_c \approx 0.1532$ GeV and the pseudocritical temperature $T_{cp} \approx 0.1537$ GeV at $\mu_I = 0$, respectively.

With the boundary conditions Eqs. (17) and (18), we can solve Eq. (16) by "shooting method" [90] and extract the chiral condensate σ as a function of temperature T or isospin chemical potential μ_I. The relevant numerical results are presented in Fig. 1.

In model I, the result shows that the chiral condensate σ decreases monotonously with the increasing of temperature in chiral limit and with physical quark mass. In chiral limit, σ vanishes at the critical temperature T_c (at $\mu_I = 0$, $T_c \approx 0.163$ GeV). With finite physical quark mass ($m_q = 3.22$ MeV) and zero isospin chemical potential, however, the second-order phase transition becomes a crossover with the pseudocritical temperature $T_{cp} \approx 0.164$ GeV.[2] In model II, the critical temperature T_c approximately equals 0.1532 GeV in chiral limit. The pseudocritical temperature T_{cp} approximately equals 0.1537 GeV at $\mu_I = 0$ with physical quark mass $m_q = 3.58$ MeV. We find that with the increasing of μ_I, the curve of σ shifts toward the sigma axis, which suggests the fact that isospin chemical potential tends to destroy the chiral symmetry.

III. CORRELATION FUNCTIONS AND MASS OF PIONS AT FINITE TEMPERATURE AND ISOSPIN DENSITY

In the previous section, we have briefly reviewed the soft-wall AdS/QCD model and obtained the temperature dependent behavior of chiral condensate at different μ_I. In this section, we will calculate screening masses and pole masses, as well as thermal widths of pions at finite isospin density and temperature, from which one can obtain the information of pion superfluid phase transition at finite temperature.

[2]The pseudocritical temperature T_{cp} is defined by $d^2\sigma(T)/dT^2|_{T=T_{cp}} = 0$.

The screening mass $m_{\rm scr}$ is defined as the exponential decay of spatial correlator, i.e., the inverse of the correlation length $\xi \sim 1/m_{\rm scr}$. In momentum space, it corresponds to the pole of the retarded correlator,

$$G(\boldsymbol{p}) \sim \frac{1}{\boldsymbol{p}^2 + m_{\rm scr}^2}, \tag{19}$$

with the frequency $\omega = 0$. As for the pole mass $m_{\rm pole}$ and the thermal width Γ, they are the real and imaginary part of frequency ($\omega_0 = m_{\rm pole} - i\Gamma/2$) of the corresponding QNM, which is the pole of the temporal retarded correlator in frequency space,

$$G(\omega) \sim \frac{1}{\omega - (m_{\rm pole} - i\Gamma/2)}, \tag{20}$$

with the momentum $\mathbf{p} = \mathbf{0}$.

Holographic approach, connecting the 4D operator $\hat{O}(x)$ and 5D field $\phi(x, z)$ through the equivalence of the partition functions, provides a powerful tool to calculate the strong coupling correlation function, namely

$$\langle e^{i\int d^4x \phi_0(x)\hat{O}(x)} \rangle = e^{iS_{5D}[\phi]}|_{\phi(x,z=0)=\phi_0(x)}, \tag{21}$$

where ϕ is the classical solution of the 5D action S_{5D} and its boundary value $\phi(x, z = 0)$ equals the 4D external source $\phi_0(x)$ [36–38]. By taking second derivative of the action S_{5D} with respect to the source ϕ_0, one can obtain the correlator $\langle \hat{O}(x)\hat{O}(0)\rangle$ [91].

A. Pseudoscalar channel

In this part, we will derive the spatial correlation functions as well as the temporal correlation functions for the pseudoscalar mesons. In 4D quantum field theory, particles are recognized as the excitation modes of the vacuum, while they are the perturbations on the background fields in the dual 5D gravity theory. For the pions, we have

$$X = \frac{\mathrm{I}}{2}\chi e^{2i\pi^a t^a}, \tag{22}$$

where I is a two-dimensional identity matrix and π^a (a = 1, 2, 3) is the pion perturbation. Here, we have neglected other channel perturbations which do not affect our discussion. Substituting Eq. (22) into Eq. (1) and keeping the quadratic terms, together with the gauge condition $A_z = 0$, one can obtain the action of pseudoscalar part as

$$\begin{aligned} S_{PS} = \int d^4x \int_0^{z_h} dz\sqrt{g}e^{-\Phi}\Big\{\frac{1}{2}(M_A^2)_{ab}[g^{zz}\partial_z\pi^a\partial_z\pi^b \\ + g^{\mu\nu}\partial_\mu\pi^a\partial_\nu\pi^b - 2g^{\mu\nu}\partial_\mu\pi^a A_\nu^b + g^{\mu\nu}A_\mu^a A_\nu^b] \\ + g^{tt}\Big[\frac{1}{2}\nu(z)^2(M_D^2)_{ab}\pi^a\pi^b + \nu(z)(M_I^2)_{ab}(\pi^b\partial_t\pi^a \\ + \pi^a A_t^b)\Big] - \frac{1}{2g_5^2}g^{zz}g^{\mu\nu}\partial_z A_\mu^a\partial_z A_\nu^a - \frac{1}{2g_5^2}g^{tt}g^{ii} \\ \times(\partial_t A_i^a - \partial_i A_t^a)^2\Big\}, \end{aligned} \tag{23}$$

where $(M_A^2)_{ab}$, $(M_I^2)_{ab}$, and $(M_D^2)_{ab}$ are 3×3 matrices defined as follows,

$$(M_A^2)_{ab} = \begin{pmatrix} \chi^2 & 0 & 0 \\ 0 & \chi^2 & 0 \\ 0 & 0 & \chi^2 \end{pmatrix}, \tag{24a}$$

$$(M_I^2)_{ab} = \begin{pmatrix} 0 & -\chi^2 & 0 \\ \chi^2 & 0 & 0 \\ 0 & 0 & 0 \end{pmatrix}, \tag{24b}$$

$$(M_D^2)_{ab} = \begin{pmatrix} \chi^2 & 0 & 0 \\ 0 & \chi^2 & 0 \\ 0 & 0 & 0 \end{pmatrix}, \tag{24c}$$

with a, b the generator indexes of SU(2). Here, π^a and A_μ^a are functions of the coordinates $x = (t, -\boldsymbol{x})$ and z. By taking the Fourier transformations,

$$\pi^a(x,z) = \frac{1}{(2\pi)^4}\int d^4k e^{ikx}\pi^a(k,z), \tag{25a}$$

$$A_\mu^a(x,z) = \frac{1}{(2\pi)^4}\int d^4k e^{ikx}A_\mu^a(k,z), \tag{25b}$$

one can solve the equation of motions in momentum space $k = (\omega, -\boldsymbol{p})$. Without losing generality and for simplicity, we assign $\boldsymbol{p}$ along the x_1-direction, i.e., $\boldsymbol{p} = (p, 0, 0)$. Due to the isospin symmetry breaking at finite isospin chemical potential, the neutral pion π^3 and the charged pions $\pi^{1,2}$ will no longer be degenerate. Thus, we have to take the isospin index ($a = 1, 2, 3$) into account. For convenience, we define $\pi^3 = \pi^0$, and take a rotation in isospin space,

$$\begin{pmatrix} \pi^1 \\ \pi^2 \end{pmatrix} = \begin{pmatrix} \frac{1}{\sqrt{2}} & \frac{1}{\sqrt{2}} \\ \frac{i}{\sqrt{2}} & -\frac{i}{\sqrt{2}} \end{pmatrix}\begin{pmatrix} \pi^+ \\ \pi^- \end{pmatrix}, \tag{26a}$$

$$\begin{pmatrix} A_t^1 \\ A_t^2 \end{pmatrix} = \begin{pmatrix} \frac{1}{\sqrt{2}} & \frac{1}{\sqrt{2}} \\ \frac{i}{\sqrt{2}} & -\frac{i}{\sqrt{2}} \end{pmatrix}\begin{pmatrix} A_t^+ \\ A_t^- \end{pmatrix}. \tag{26b}$$

From the action in Eq. (23), the EOMs of π^0, A_t^0, and A_i^0 are derived as

$$\begin{aligned} \pi^{0\prime\prime} + \Big(3A' - \Phi' + \frac{f'}{f} + 2\frac{\chi'}{\chi}\Big)\pi^{0\prime} \\ + \Big(\frac{\omega^2}{f^2} - \frac{p^2}{f}\Big)\pi^0 - \frac{i\omega}{f^2}A_t^0 - \frac{ip}{f}A_i^0 = 0, \end{aligned} \tag{27a}$$

$$\begin{aligned} A_t^{0\prime\prime} + (A' - \Phi')A_t^{0\prime} - \frac{g_5^2 e^{2A}\chi^2 i\omega}{f}\pi^0 \\ - \frac{p^2 + g_5^2 e^{2A}\chi^2}{f}A_t^0 - \frac{\omega p}{f}A_i^0 = 0, \end{aligned} \tag{27b}$$

$$\begin{aligned} A_i^{0\prime\prime} + \Big(A' - \Phi' + \frac{f'}{f}\Big)A_i^{0\prime} + \frac{g_5^2 e^{2A}\chi^2 ip}{f}\pi^0 \\ + \frac{\omega^2 - fg_5^2 e^{2A}\chi^2}{f^2}A_i^0 + \frac{\omega p}{f^2}A_t^0 = 0, \end{aligned} \tag{27c}$$

and the EOMs of $\pi^\pm$, $A_t^\pm$, and $A_i^\pm$ are derived as

$$\begin{aligned} \pi^{\pm\prime\prime} + \Big(3A' - \Phi' + \frac{f'}{f} + 2\frac{\chi'}{\chi}\Big)\pi^{\pm\prime} + \frac{(\omega\pm\nu)^2 - fp^2}{f^2}\pi^\pm \\ - \frac{i(\omega\pm\nu)}{f^2}A_t^\pm - \frac{ip}{f}A_i^\pm = 0, \end{aligned} \tag{28a}$$

$$\begin{aligned} A_t^{\pm\prime\prime} + (A' - \Phi')A_t^{\pm\prime} - \frac{g_5^2 e^{2A}\chi^2 i(\omega\pm\nu)}{f}\pi^\pm \\ - \frac{p^2 + g_5^2 e^{2A}\chi^2}{f}A_t^\pm - \frac{\omega p}{f}A_i^\pm = 0, \end{aligned} \tag{28b}$$

$$\begin{aligned} A_i^{\pm\prime\prime} + \Big(A' - \Phi' + \frac{f'}{f}\Big)A_i^{\pm\prime} + \frac{g_5^2 e^{2A}\chi^2 ip}{f}\pi^\pm \\ + \frac{\omega^2 - fg_5^2 e^{2A}\chi^2}{f^2}A_i^\pm + \frac{\omega p}{f^2}A_t^\pm = 0, \end{aligned} \tag{28c}$$

where the prime represents the derivative with respect to z.

Note that the EOMs are coupled linear second-order differential equations with double singularities. The analytical solutions are almost impossible to get. Therefore, we have to solve them numerically. Since the structure of the asymptotic expansion solutions and the relative numerical algorithm are the same for solving the EOMs of pions in these two soft-wall AdS/QCD models, we only give the numerical details for model I in this subsection. We can get the asymptotic expansions of π^0, A_t^0, and A_i^0 at the UV boundary,[3]

$$\pi^0(z \to 0) = \pi_0 + \frac{1}{2}[\pi_0(p^2 - \omega^2) + i(\varphi_0 p + a_0\omega)] \times z^2 \ln(z) + \pi_2 z^2 + \mathcal{O}(z^3), \tag{29a}$$

$$A_t^0(z \to 0) = a_0 + \frac{1}{2}[a_0(p^2 + g_5^2 m_q^2 \zeta^2) + \varphi_0 p\omega + i g_5^2 m_q^2 \zeta^2 \pi_0 \omega] z^2 \ln(z) + a_2 z^2 + \mathcal{O}(z^3), \tag{29b}$$

$$A_i^0(z \to 0) = \varphi_0 + \frac{1}{2}[p(-i g_5^2 m_q^2 \zeta^2 \pi_0 - a_0\omega) + \varphi_0(g_5^2 m_q^2 \zeta^2 - \omega^2)] z^2 \ln(z) + \varphi_2 z^2 + \mathcal{O}(z^3), \tag{29c}$$

where π_0, π_2, a_0, a_2, φ_0, φ_2 are free undetermined integration constants. According to the holographic dictionary, π_0, a_0, φ_0 correspond to the external sources J_π, J_{A_t}, and J_{A_i}, respectively. At the horizon, we can also get the asymptotic expansions as[4]

$$\pi^0(z \to z_h) = (z_h - z)^{\frac{i\omega z_h}{2\mu_I^2 z_h^2 - 4}}\{\pi_{h0} + \pi_{h1}(z - z_h) + \mathcal{O}[(z - z_h)^2]\} + b_{h0} + \frac{i b_{h1} z_h^2 \omega (z - z_h)}{16 + 4 z_h^4 \mu_I^4 + z_h^2(-16\mu_I^2 + \omega^2)} + \mathcal{O}[(z - z_h)^2], \tag{30a}$$

$$A_t^0(z \to z_h) = (z_h - z)^{\frac{i\omega z_h}{2\mu_I^2 z_h^2 - 4}}\{a_{h1}(z - z_h) + \mathcal{O}[(z - z_h)^2]\} - i b_{h0}\omega + b_{h1}(z - z_h) + \mathcal{O}[(z - z_h)^2], \tag{30b}$$

$$A_i^0(z \to z_h) = (z_h - z)^{\frac{i\omega z_h}{2\mu_I^2 z_h^2 - 4}}\left\{-i\left[\frac{2\pi_{h0} c_0^2 g_5^2(-2 + z_h^2\mu_I^2)}{2p z_h^2(-2 + z_h^2\mu_I^2)} + \frac{a_{h1} z_h^2(4 - 2z_h^2\mu_I^2 - i z_h\omega)}{2p z_h^2(-2 + z_h^2\mu_I^2)}\right] + \varphi_{h1}(z - z_h) + \mathcal{O}[(z - z_h)^2]\right\} + i b_{h0} p - \frac{b_{h1} p z_h^2 \omega (z - z_h)}{16 + 4 z_h^4 \mu_I^4 + z_h^2(-16\mu_I^2 + \omega^2)} + \mathcal{O}[(z - z_h)^2] \tag{30c}$$

with coefficients of first order in Eq. (31),

$$\begin{aligned}\pi_{h1} = {}& \{-2a_{h1} z_h^2(-2 + z_h^2\mu_I^2)^2 + \pi_{h0} c_0^2(-2 + z_h^2\mu_I^2) \\ & \times [2g_5^2(-2 + z_h^2\mu_I^2) - i z_h \lambda\omega] \\ & + \pi_{h0} z_h^2\{2p^2(-2 + z_h^2\mu_I^2)^2 + i\omega[4z_h^5\mu_g^2\mu_I^4 \\ & + z_h^3\mu_I^2(2\mu_c^2 - 16\mu_g^2 - 3\mu_I^2) + z_h(-4\mu_c^2 \\ & + 16\mu_g^2 + 6\mu_I^2) + 6i\omega - 9i z_h^2 \mu_I \omega]\}\}/[4z_h(-2 \\ & + z_h^2\mu_I^2)^2(-2 + z_h^2\mu_I^2 + i z_h\omega)],\end{aligned} \tag{31a}$$

$$\begin{aligned}\varphi_{h1} = {}& i\{-4\pi_{h0} c_0^2 g_5^2 p^2 z_h^2(-2 + z_h^2\mu_I^2)^3 + 2i a_{h1} p^2 z_h^5(-2 \\ & + z_h^2\mu_I^2)^2\omega + [-2\pi_{h0} c_0^2 g_5^2(-2 + z_h^2\mu_I^2) + a_{h1} z_h^2(-4 \\ & + 2z_h^2\mu_I^2 + i z_h\omega)][2c_0^2 g_5^2(-2 + z_h^2\mu_I^2)^2 + i z_h\omega(-4 \\ & + 4z_h^6\mu_g^2\mu_I^4 + 16 z_h^2(\mu_g^2 + \mu_I^2) - z_h^4(16\mu_g^2\mu_I^2 + 7\mu_I^4) \\ & + 6i z_h\omega - 9i z_h^3\mu_I^2\omega)]\}/\left\{8z_h^3(-2 + z_h^3\mu_I^2)^4 \right. \\ & \left. \times\left(p + \frac{i p z_h\omega}{-2 + z_h^2\mu_I^2}\right)\right\},\end{aligned} \tag{31b}$$

where π_{h0}, a_{h1}, b_{h0}, and b_{h1} are independent integration constants. As for the EOMs of $\pi^\pm$, $A_t^\pm$ and $A_i^\pm$, i.e., Eqs. (28a)–(28c), we can also obtain the UV boundary asymptotic expansions as

$$\pi^\pm(z \to 0) = \pi_0^\pm + \frac{1}{2}\{i\varphi_0^\pm p + i a_0^\pm(\omega \pm \mu_I) + \pi_0^\pm(p^2 - (\omega \pm \mu_I)^2)\} z^2 \ln(z) + \pi_2^\pm z^2 + \mathcal{O}(z^3), \tag{32a}$$

$$A_t^\pm(z \to 0) = a_0^\pm + \frac{1}{2}\{a_0^\pm(p^2 + g_5^2 m_q^2\zeta^2) + \varphi_0^\pm p\omega + i g_5^2 m_q^2 \zeta^2 \pi_0^\pm(\omega \pm \mu_I)\} \times z^2 \ln(z) + a_2^\pm z^2 + \mathcal{O}(z^3), \tag{32b}$$

$$A_i^\pm(z \to 0) = \varphi_0^\pm + \frac{1}{2}\{\varphi_0^\pm g_5^2 m_q^2 \zeta^2 - i g_5^2 m_q^2 p \zeta^2 \pi_0^\pm - a_0^\pm p\omega - \varphi_0^\pm \omega^2\} z^2 \ln(z) + \varphi_2^\pm z^2 + \mathcal{O}(z^3), \tag{32c}$$

[3]These are generalized regular series expansions and what we just require is that π^0, A_t^0, and A_i^0 are not divergent at $z \to 0$. The same regular conditions must also be met in the following series expansions.

[4]Here, we take the incoming wave solution and neglect the outgoing one.

where $\pi_0^\pm$, $\pi_2^\pm$, $a_0^\pm$, $a_2^\pm$, $\varphi_0^\pm$, $\varphi_2^\pm$ are independent integration constants. Similarly, the horizon asymptotic expansions read

$$\begin{aligned}\pi^\pm(z\to z_h) &= (z_h-z)^{\frac{i\omega z_h}{2\mu_I^2 z_h^2-4}}\{\pi_{h0}^\pm+\pi_{h1}^\pm(z-z_h)\\&\quad+\mathcal{O}[(z-z_h)^2]\}+b_{h0}^\pm\\&\quad+\frac{(z-z_h)z_h(ib_{h1}^\pm z_h\pm 2b_{h0}^\pm\mu_I)\omega}{16+4z_h^4\mu_I^4+z_h^2(-16\mu_I^2+\omega^2)}\\&\quad+\mathcal{O}[(z-z_h)^2],\end{aligned}\tag{33a}$$

$$\begin{aligned}A_t^\pm(z\to z_h) &= (z_h-z)^{\frac{i\omega z_h}{2\mu_I^2 z_h^2-4}}\{a_{h1}^\pm(z-z_h)+\mathcal{O}[(z-z_h)^2]\}\\&\quad-ib_{h0}^\pm\omega+b_{h1}^\pm(z-z_h)+\mathcal{O}[(z-z_h)^2],\end{aligned}\tag{33b}$$

$$\begin{aligned}A_i^\pm(z\to z_h) &= (z_h-z)^{\frac{i\omega z_h}{2\mu_I^2 z_h^2-4}}\Bigg\{-i\Bigg[\frac{2\pi_{h0}^\pm c_0^2 g_5^2(-2+z_h^2\mu_I^2)}{2pz_h^2(-2+z_h^2\mu_I^2)}\\&\quad+\frac{a_{h1}^\pm z_h^2(4-2z_h^2\mu_I^2-iz_h\omega)}{2pz_h^2(-2+z_h^2\mu_I^2)}\Bigg]\\&\quad+\varphi_{h1}^\pm(z-z_h)+\mathcal{O}[(z-z_h)^2]\Bigg\}\\&\quad+ib_{h0}^\pm p-\frac{b_{h1}^\pm p z_h^2\omega(z-z_h)}{16+4z_h^4\mu_I^4+z_h^2(-16\mu_I^2+\omega^2)}\\&\quad+\mathcal{O}[(z-z_h)^2]\end{aligned}\tag{33c}$$

with coefficients of first order in Eq. (34),

$$\begin{aligned}\pi_{h1}^\pm &= \{-2a_{h1}^\pm z_h^2(-2+z_h^2\mu_I^2)^2+\pi_{h0}^\pm c_0^2(-2+z_h^2\mu_I^2)\\&\quad\times[2g_5^2(-2+z_h^2\mu_I^2)-iz_h\lambda\omega]\\&\quad+\pi_{h0}^\pm z_h^2\{2p^2(-2+z_h^2\mu_I^2)^2+i\omega[4z_h^5\mu_g^2\mu_I^4\\&\quad+z_h^3\mu_I^2(2\mu_c^2-16\mu_g^2-3\mu_I^2)+z_h(-4\mu_c^2+16\mu_g^2\\&\quad+6\mu_I^2)+2i(4\mu_I+3\omega)-iz_h^2\mu_I^2(4\mu_I+9\omega)]\}\}\\&\quad/[4z_h(-2+z_h^2\mu_I^2)^2(-2+z_h^2\mu_I^2+iz_h\omega)],\end{aligned}\tag{34a}$$

$$\begin{aligned}\varphi_{h1}^\pm &= i\{-4\pi_{h0}^\pm c_0^2 g_5^2 p^2 z_h^2(-2+z_h^2\mu_I^2)^3+2ia_{h1}^\pm p^2 z_h^5(-2\\&\quad+z_h^2\mu_I^2)^2\omega+[-2\pi_{h0}^\pm c_0^2 g_5^2(-2+z_h^2\mu_I^2)+a_{h1}^\pm z_h^2(-4\\&\quad+2z_h^2\mu_I^2+iz_h\omega)][2c_0^2g_5^2(-2+z_h^2\mu_I^2)^2+iz_h\omega(-4\\&\quad+4z_h^6\mu_g^2\mu_I^4+16z_h^2(\mu_g^2+\mu_I^2)-z_h^4(16\mu_g^2\mu_I^2+7\mu_I^4)\\&\quad+6iz_h\omega-9iz_h^3\mu_I^2\omega)]\}/\Bigg\{8z_h^3(-2+z_h^3\mu_I^2)^4\\&\quad\times\left(p+\frac{ipz_h\omega}{-2+z_h^2\mu_I^2}\right)\Bigg\},\end{aligned}\tag{34b}$$

where the independent integration constants are $\pi_{h0}^\pm$, $a_{h1}^\pm$, $b_{h0}^\pm$, and $b_{h1}^\pm$.

The on-shell action of pion is

$$\begin{aligned}S_\pi^{\text{on}} &= \frac{1}{2g_5^2}\int d^4k\sum_{a=1}^{3}\{e^{A-\Phi}[A_t^a(-k,z)\partial_z A_t^a(k,z)\\&\quad-fA_i^a(-k,z)\partial_z A_i^a(k,z)]\\&\quad-e^{3A-\Phi}g_5^2 f\chi^2\pi^a(-k,z)\partial_z\pi^a(k,z)\}|_{z=\epsilon}^{z=z_h}.\end{aligned}\tag{35}$$

Substituting the Eqs. (29)–(33) into Eq. (35) and taking derivative with respect to the source J_π, we can obtain the on-shell action and the retarded correlator of π^0 as follows

$$\begin{aligned}S_{\pi^0}^{\text{on}} &= \frac{1}{g_5^2}\int d^4k\{a_0(-k)a_2(k)-\varphi_0(-k)\varphi_2(k)\\&\quad-g_5^2m_q^2\zeta^2\pi_0(-k)\pi_2(k)+\cdots\},\end{aligned}\tag{36}$$

$$G_{\pi^0}(k)=\frac{\delta^2 S_{\pi^0}^{\text{on}}}{\delta J_{\pi^0}^*\delta J_{\pi^0}}=-m_q^2\zeta^2\frac{\pi_2(k)}{\pi_0(k)}+\cdots,\tag{37}$$

where the symbol $\cdots$ represents for some pole-irrelevant terms. From the explicit formation of retarded correlator of π^0 in Eq. (37), it is obvious that the value of the correlator at k is only dependent on the integration constants of the asymptotic expansions in Eq. (29). In principle, these integration constants can be obtained by numerically solving the EOM of π^0 in Eq. (27) with the boundary conditions in Eq. (29)–(31) through the "Shooting" method.

The on-shell action and the retarded correlator of $\pi^\pm$ read

$$\begin{aligned}S_{\pi^\pm}^{\text{on}} &= \frac{1}{g_5^2}\int d^4k\{a_0^\pm(k)^*a_2^\pm(k)-\varphi_0^\pm(k)^*\varphi_2^\pm(k)\\&\quad-g_5^2m_q^2\zeta^2\pi_0^\pm(k)^*\pi_2^\pm(k)+\cdots\},\end{aligned}\tag{38}$$

$$G_{\pi^\pm}(k)=\frac{\delta^2 S_{\pi^\pm}^{\text{on}}}{\delta J_{\pi^\pm}^*\delta J_{\pi^\pm}}=-m_q^2\zeta^2\frac{\pi_2^\pm(k)}{\pi_0^\pm(k)}+\cdots,\tag{39}$$

where the symbol $\cdots$ represents for some pole-irrelevant terms. Similar to the retarded correlator of π^0 in Eq. (37), the retarded correlators of $\pi^\pm$, $G_{\pi^\pm}$ in Eq. (39), are only dependent on the integration constants of the asymptotic expansions in Eq. (32).

B. Screening masses of pions

In this section, we will numerically solve the EOMs of pions numerically and extract screening masses from the pole of the spatial correlation functions in two different soft-wall AdS/QCD models. Then we will investigate the temperature as well as the isospin chemical potential dependence of screening masses. In this paper, we will mainly focus on the temperature region below T_{cp}. Not only does the pion condensate occur below the chiral transition temperature, but also the particles of pions are not well-defined degrees of freedom at high temperature.

For the screening mass corresponds the pole of the spatial correlator, one can let the frequency $\omega = 0$ in the EOMs, the boundary asymptotic expansions and the retarded correlators in Eqs. (27)–(39). For the neutral pion, Eqs. (27), (29)–(31) and (35)–(37), in order to obtain the pole of its spatial correlator, the corresponding integration constants in the UV asymptotic expansions in Eq. (29) should take the following conditions,[5]

$$\pi_0(p^2) = 0, \qquad a_0(p^2) = 0, \qquad \varphi_0(p^2) = 0. \quad (40)$$

When one solves the EOMs in Eq. (27), the lowest state of p^2 satisfying Eq. (40) corresponds to screening mass of the neutral pion, i.e., $m^2_{\rm scr} = -p^2$. To accomplish the numerical solving, constrains on the horizon are also essential. On the horizon, since the equations for π^0, A^0_t, and A^0_i [Eqs. (27a)–(27c)] are linear differential equations, we can set the integration constant π_{h0} to be unity ($\pi_{h0} = 1$) without shifting the mass spectra. The integration constant b_{h1} should be set to zero ($b_{h1} = 0$) which insure the on-shell action $S^{\rm on}_\pi$ is independent of horizon terms [91].[6] Finally, the remain undetermined integration constants, b_{h0} and a_{h1}, and the target momentum p^2 (i.e. the screening mass), can be determined by "shooting method" [90].

The same prescription can be also applied to the EOMs of charged pions in Eqs. (28a)–(28c). On the horizon, one can take $\pi^\pm_{h0} = 1$, while $b^\pm_{h0}$, $a^\pm_{h1}$ and p^2 can be determined by "shooting method" when the following conditions for the integration constants in the UV boundary asymptotic expansion solutions in Eq. (32) are simultaneously satisfied,

$$\pi^\pm_0(p^2) = 0, \qquad a^\pm_0(p^2) = 0, \qquad \varphi^\pm_0(p^2) = 0. \quad (41)$$

They lead to the pole of the correlator in Eq. (39). However, there are some differences from the case of π^0, which relate to the integration constant $b^\pm_{h1}$ on the horizon at finite isospin chemical potential. We find that only the condition $\partial_z\pi^\pm(z \to z_h) = 0$, i.e., $b^\pm_{h1} = \pm 2ib^\pm_{h0}\mu_I/z_h$ predicts appropriate spectra of charged pions. When $\mu_I = 0$, $b^\pm_{h1}$ reduces to zero, which is consistent with the previous discussions. Considering the boundary conditions and the physical constrains, we can also solve the EOMs and extract the screening masses of the charged pions.

[5]As a result of the coupling between the pion and the axial vector meson, Eq. (27) is not only the EOMs for the pion but also for the axial vector meson, the degree of freedoms of the pion and the axial vector meson are both encode in these coupled equations. To obtain the pole of the correlator of the axial vector meson, it requires the integration constants $a_0 = 0$ and $\varphi_0 = 0$, but π_0 undetermined.

[6]On the horizon, as to the pole of the axial vector meson, one should let $\pi_{h0} = 1$, $b_{h0} = 0$, $b_{h1} = 0$.

1. The temperature effect

The numerical results of screening masses, varying with temperature, are presented in Fig. 2. Qualitatively, one can find that these two soft-wall AdS/QCD models share the same features in predicting the temperature behavior of screening masses of pions. For π^0, the numerical results are shown in Figs. 2(a) and (b). We find that the screening mass of neutral pion at very low temperature is almost independent on T. The value of $m_{{\rm scr},\pi^0}/m_\pi$[7] gets closed to 1, which implies that the screening mass of π^0 at low temperature almost remains m_π. As the rising of T, $m_{{\rm scr},\pi^0}$ grows slowly first and then enhances quickly when T is close to the pseudocritical temperature $T_{cp}(\mu_I)$.[8] What is more, it is noteworthy that $m_{{\rm scr},\pi^0}$ at different μ_I have almost the same value. It is because that π^0 does not carry isospin charge. Consequently, the isospin chemical potential has little impact on $m_{{\rm scr},\pi^0}$.

For the screening masses of charged pions $\pi^\pm$, the numerical results at different μ_I are shown in Figs. 2(c) and (d). At finite isospin chemical potential, we find that the screening masses of π^+ and π^- are degenerate, which is in agreement with the NJL model results in Ref. [30]. From the NJL studies in Refs. [29,30], it can be seen that the charged pions share the same isospin chemical potential dependence in the mesoic propagator when $\omega = 0$, i.e., the charged pions feel the same spatial effect of the medium, which leads to the degenerate of the screening masses of the charged pions. In our holographic models, when one lets the frequency $\omega = 0$ in the EOMs of charged pions, in Eq. (28), it is obviously that the EOMs reduce to the same. Therefore, screening masses of charged pions are degenerate. With the increasing of temperature, the screening masses increase. However, with the increasing of isospin chemical potential, the screening masses decrease. For example, we can see in both models that at fixed temperature $T/T_{cp}(\mu_I) = 0.4$,

$$m_{{\rm scr},\pi^\pm}(\mu_I = 0.01\ {\rm GeV}) \approx m_\pi,$$
$$m_{{\rm scr},\pi^\pm}(\mu_I = 0.05\ {\rm GeV}) \approx 0.95m_\pi,$$
$$m_{{\rm scr},\pi^\pm}(\mu_I = 0.10\ {\rm GeV}) \approx 0.8m_\pi.$$

Furthermore, in the high temperature region, the effect of μ_I is much weaker than the temperature effect. Therefore, the curves become degenerate when T closes to T_{cp}.

To compare the screening masses between the neutral and charged pions, we show the temperature dependence of the screening masses at fixed isospin chemical potential

[7]Here, $m_\pi \approx 0.13971136$ GeV, which is the pion mass at $T = 0$, $\mu_I = 0$ in model I [55], and $m_\pi \approx 0.13971648$ GeV in model II.

[8]From the discussion in Sec. II, it can be seen that T_{cp} is affected by μ_I. It is found that $T_{cp}(\mu_I)$ will decrease as the rising of μ_I.

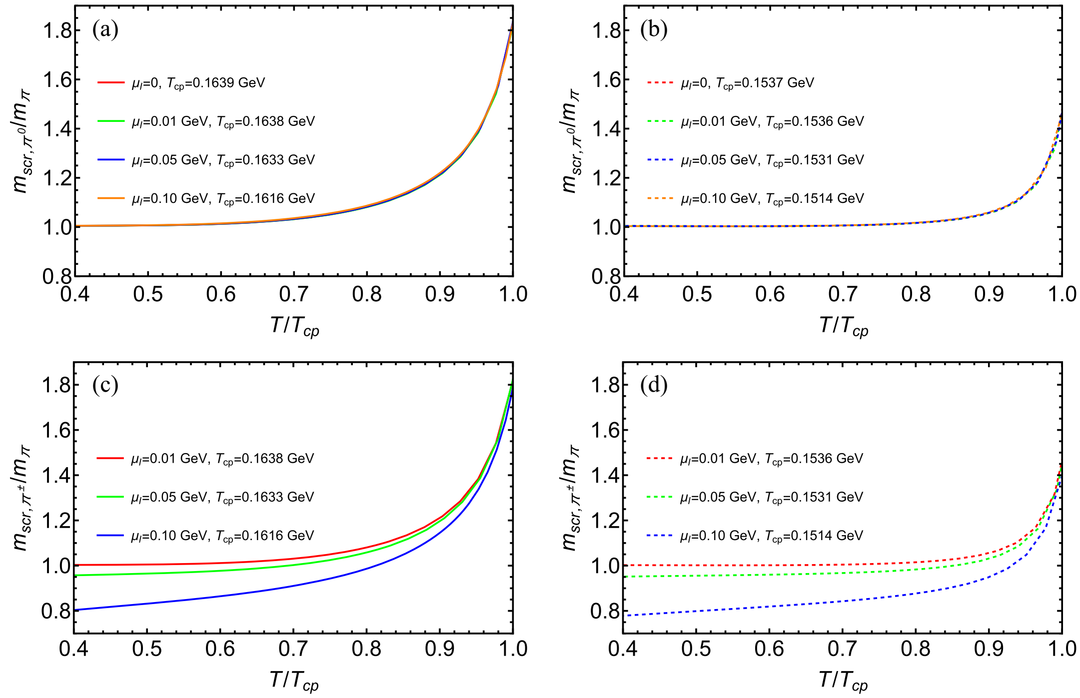

FIG. 2. Screening masses as functions of T for π^0 in (a) model I and (b) model II. The red, green, blue, and orange solid lines stand for the results below T_{cp}, at $\mu_I = 0, 0.01, 0.05, 0.10$ GeV, respectively. Screening masses as functions of T for charged pions $\pi^\pm$ in (c) model I and (d) model II. The red, green,and blue solid lines stand for the results below T_{cp}, at $\mu_I = 0.01, 0.05, 0.10$ GeV, respectively.

$\mu_I = 0.10$ GeV in Figs. 3. In both models, the screening mass of π^0 gets close to m_π, while $\pi^\pm$ is about $0.8 m_\pi$ at low temperature. However, they become degenerate at relatively high temperatures, which implies that the effect of isospin chemical potential can be neglected.

2. The isospin density effect

After considering the temperature dependence of the screening masses at fixed isospin chemical potential, we will discuss the effect of isospin chemical potential on screening masses at fixed temperatures in this subsection. Due to the qualitative consistency of the conclusions obtained at different temperatures, we only choose the fixed temperature $T = 0.10$ GeV for the discussion without loss of generality. The numerical results of the isospin chemical potential dependence of the screening masses in both models are presented in Fig. 4. Both of these models exhibit the same behaviors. In the normal phase, i.e., $\mu_I < \mu_I^c$, m_{scr,π^0} and $m_{\mathrm{scr},\pi^\pm}$ are splitting. It may be reasonable that the EOMs, in Eq. (28), of charged pions depend on isospin density, but the neutral ones, in Eq. (27), do not. The neutral pion π^0 almost keeps unchanged with the increasing of isospin chemical potential. This is consistent with the previous discussion since π^0 does not carry isospin charge. What is more, $m_{\mathrm{scr},\pi^\pm}$ decrease monotonically and vanish at a critical chemical potential μ_I^c, where

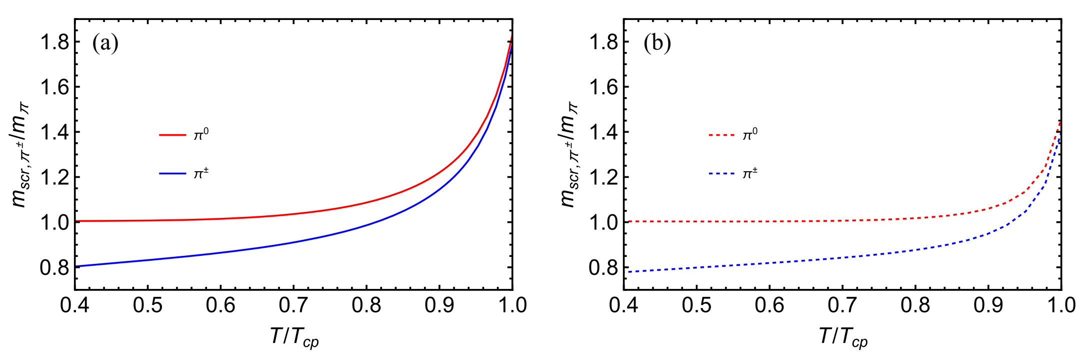

FIG. 3. Screening masses as functions of T for π^0 as well as $\pi^\pm$ in (a) model I and (b) model II at fixed isospin chemical potential $\mu_I = 0.10$ GeV.

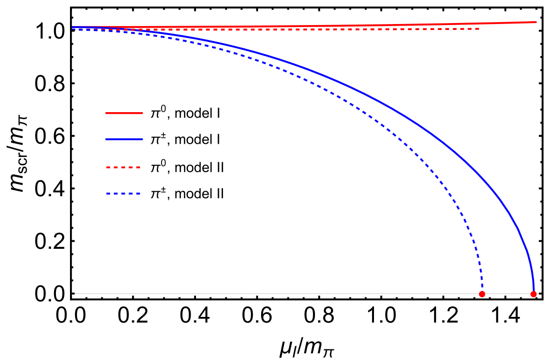

FIG. 4. Screening masses as functions of isospin chemical potential μ_I at fixed temperature $T = 0.10$ GeV in model I (solid lines) and model II (dashed lines). The red and blue lines stand for π^0 and $\pi^\pm$, respectively. Screening masses of charged pions m_{scr} vanish at 1.49 $m_\pi \approx 0.208$ GeV in model I and 1.32 $m_\pi \approx$ 0.184 GeV in model II, as shown by the red dots.

the pion superfluid phase transition occurs. For the chosen temperature $T = 0.10$ GeV, the critical isospin chemical potential μ_I^c in model I is about $1.49 m_\pi \approx 0.208$ GeV. For model II, it is $1.31 m_\pi \approx 0.183$ GeV. When the chemical potential is beyond μ_I^c, the pion condensation will happen. The discussions of pions' properties in the pion superfluid phase will be left to our future works.

Qualitatively, both of these two different soft-wall AdS/QCD models possess the same behaviors of the screening masses. Furthermore, these behaviors are well consistent with the results of the NJL model in Ref. [30].

C. Pole masses of pions

In the framework of holographic approach, one can obtain the pole masses of pions from the peaks of spectral functions which are related to the imaginary part of the two-point retarded correlation functions. However, as pointed out by our previous works [67,68], the thermal widths of quasiparticle pions will also increase with the increasing temperature, which leads to inconspicuous resonance peaks of the spectral functions. A more straightforward and effective approach is to define the effective masses of the pions through the corresponding QNM. The quasinormal frequency ω_0 corresponds to the pole of the temporal retarded correlator $G(\omega)$. Its real and imaginary parts correspond to the meson's pole mass m_{pole} and thermal width Γ, respectively, by the relation $\omega_0 = m_{\mathrm{pole}} - i\Gamma/2$.

We will numerically calculate the QNM frequencies in two different soft-wall AdS/QCD models. Herein, we just focus on the temporal retarded correlators. One can let $p = 0$, i.e. $k = (\omega, 0, 0, 0)$, in the EOMs of pion in Eqs. (27) and (28) and boundary conditions in Eqs. (29)–(34). Note that the equations of A_i^a are decoupled from π^a and A_t^a at $p = 0$. Therefore, we can neglect the equations of A_i^a and solve the ones of π^a and A_t^a only. In order to determine the particular QNM frequency, $\omega = \omega_0$, which corresponds to the pole of the retarded correlator, Eqs. (37) and (39), the integration constants in Eqs. (29) and (33) should satisfy the following conditions,

$$\pi_0(\omega = \omega_0) = a_0(\omega = \omega_0) = 0 \tag{42}$$

for the neutral pion, and

$$\pi_0^\pm(\omega = \omega_0) = a_0^\pm(\omega = \omega_0) = 0 \tag{43}$$

for the charged pions. At the horizon, the conditions of integration constants of the asymptotic expansion solutions are similar to our previous discussions for the screening mass in Sec. III B, one has

$$\pi_{h0} = 1, \qquad b_{h1} = 0 \tag{44}$$

for the neutral pion, and

$$\pi_{h0}^\pm = 1, \qquad b_{h1}^\pm = \pm 2 i b_{h0}^\pm \mu_I / z_h \tag{45}$$

for the charged pions. With these constrain conditions for the integration constants of the asymptotic expansion solutions, one can numerically solve the EOMs and obtain the QNM through "shooting method."

1. The temperature effect

To investigate the temperature dependence of pole masses and thermal widths of π^0, π^+, and π^- in two models, we fix isospin chemical potential and vary temperature. As illustrated in Sec. III B, we just pay close attention to the pole masses of pions in the normal phase at the temperature $T < T_{cp}$. We consider the cases at fixed isospin chemical potential $\mu_I = 0$, 0.01, 0.05, and 0.10 GeV, respectively. The corresponding numerical results are shown in Fig. 5. In Fig. 5(a), the pole masses m_{pole} decrease monotonously with the increasing of temperature. We have

$$\text{Model I} \quad m_{\mathrm{pole},\pi^0}(T = T_{cp}) \approx 40\% m_\pi,$$
$$\text{Model II} \quad m_{\mathrm{pole},\pi^0}(T = T_{cp}) \approx 70\% m_\pi,$$

where m_π is the model dependent pole mass with $\mu_I = 0$ and $T = 0$. Qualitatively, the decreasing behavior around the pseudocritical temperature in both soft-wall AdS/QCD models, are consistent with T. D. Son *et al.*'s analytical analysis through the chiral perturbation theory in Refs. [22,23]. In Fig. 5(b), the thermal widths Γ increase monotonously with the increasing of temperature. One can see that the results for π^0 are almost not affected by μ_I, because it does not carry isospin charge.

The results for π^+ at different fixed isospin chemical potential, are shown in Figs. 5(c) and (d). From Fig. 5(c), we find that μ_I depresses the pole mass of π^+, i.e., the larger

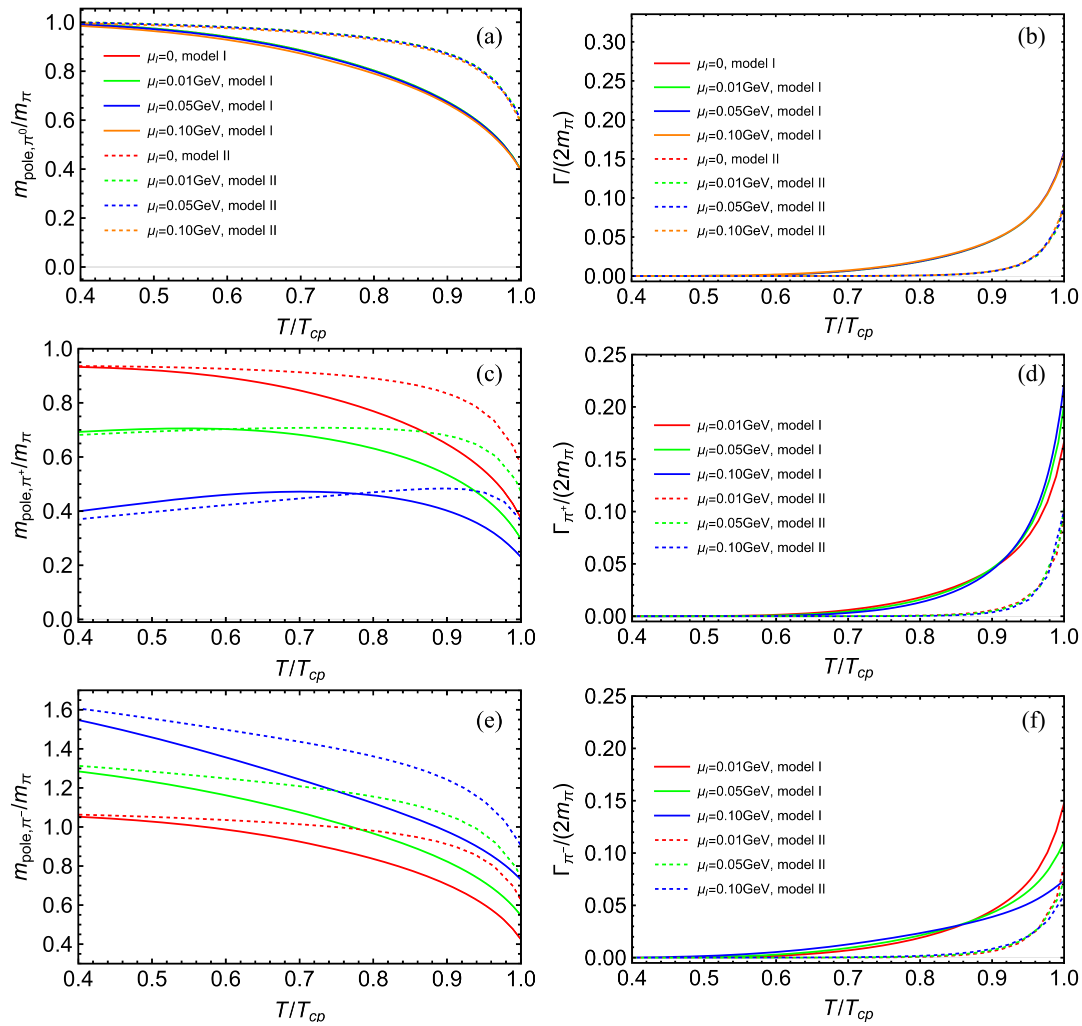

FIG. 5. Pole masses and thermal widths as functions of T for (a), (b) π^0; (c), (d) π^+, and (e), (f) π^-. In (a) and (b), the red, green, blue and orange lines stand for results at $\mu_I = 0$, 0.01, 0.05, and 0.10 GeV, respectively. In (c),(d),(e) and (f), the red, green and blue lines represent results at $\mu_I = 0.01$, 0.05 and 0.10 GeV, respectively. Model I and II are labeled by the solid and dashed lines respectively.

μ_I the lower m_{pole,π^+}. For example, at $T/T_{cp} = 0.4$, the reductions of m_{pole,π^+} at $\mu_I = 0.05$ GeV and 0.10 GeV are about 30% and 60%, respectively. This result may be reasonable since one might expect the gathering of positive isospin charge would make it easier to excite a π^+. When μ_I is small, such as $\mu_I = 0.01$ GeV, m_{pole,π^+} decreases monotonously with the increasing of temperature. However, when μ_I getting larger, such as $\mu_I = 0.10$ GeV, m_{pole,π^+} increases first at low temperature and decreases when temperature is close to $T_{cp}(\mu_I)$. In Fig. 5(d), the thermal widths of π^+ at different fixed μ_I increase very slowly and the effect of μ_I is not obvious at low temperature. When T gets close to T_{cp}, it increases quickly.

As for the negative charged pions π^-, the numerical results of the pole masses m_{pole,π^-} and thermal widths Γ_{π^-} are presented in Figs. 5(e) and (f). From the results, we can find that m_{pole,π^-} decreases monotonously with the increasing of temperature. At a fixed temperature, m_{pole,π^-} is enhanced by μ_I. For example, at $T/T_{cp} = 0.4$ GeV and $\mu_I = 0.10$ GeV, m_{pole,π^-} is increased by about 55% m_π in model I and 60% m_π in model II, respectively. While the thermal width increases with the increasing of temperature.

We show the pole masses and thermal widths of π^0, π^+, π^- at fixed $\mu_I = 0.10$ GeV in Fig. 6. At finite isospin chemical potential, the $SU_I(2)$ symmetry is explicitly broken leading to the splitting of pole masses ($m_{\text{pole},\pi^-} > m_{\text{pole},\pi^0} > m_{\text{pole},\pi^+}$).[9] As the temperature reaches

[9]From the NJL studies in Refs. [29,30], the frequency ω in the propagator for charged pions is coupled with isospin chemical potential μ_I as $(\omega \pm \mu_I)^2$. The different signs would lead to different pole masses. It is interesting that the 5D holographic model can directly derive similar conclusions. From Eq. (28), one can find coupled term $\omega \pm \nu$ with $\nu = \mu_I(z - z^2/z_h^2)$, in the EOMs of charged pions. Therefore, charged pions have different pole masses at finite μ_I.

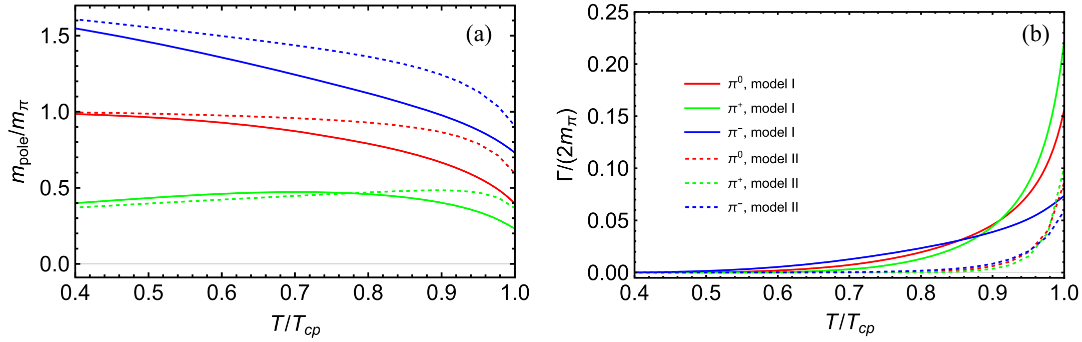

FIG. 6. (a) Pole masses and (b) thermal widths as function of T at $\mu_I = 0.10$ GeV. The blue, red and green lines represent results for π^-, π^0, π^+, respectively. The solid lines stand for results in model I and dashed lines stand for results in model II.

T_{cp}, the pole masses decrease and tend to be degenerate due to the restoration of the chiral symmetry. It can also be seen that the thermal widths increase with the increasing of temperature.

2. The isospin density effect

In this subsection, we will study the isospin chemical potential effects on pole masses and thermal widths of pions. As shown in Figs. 7(a) and (b), both models have the

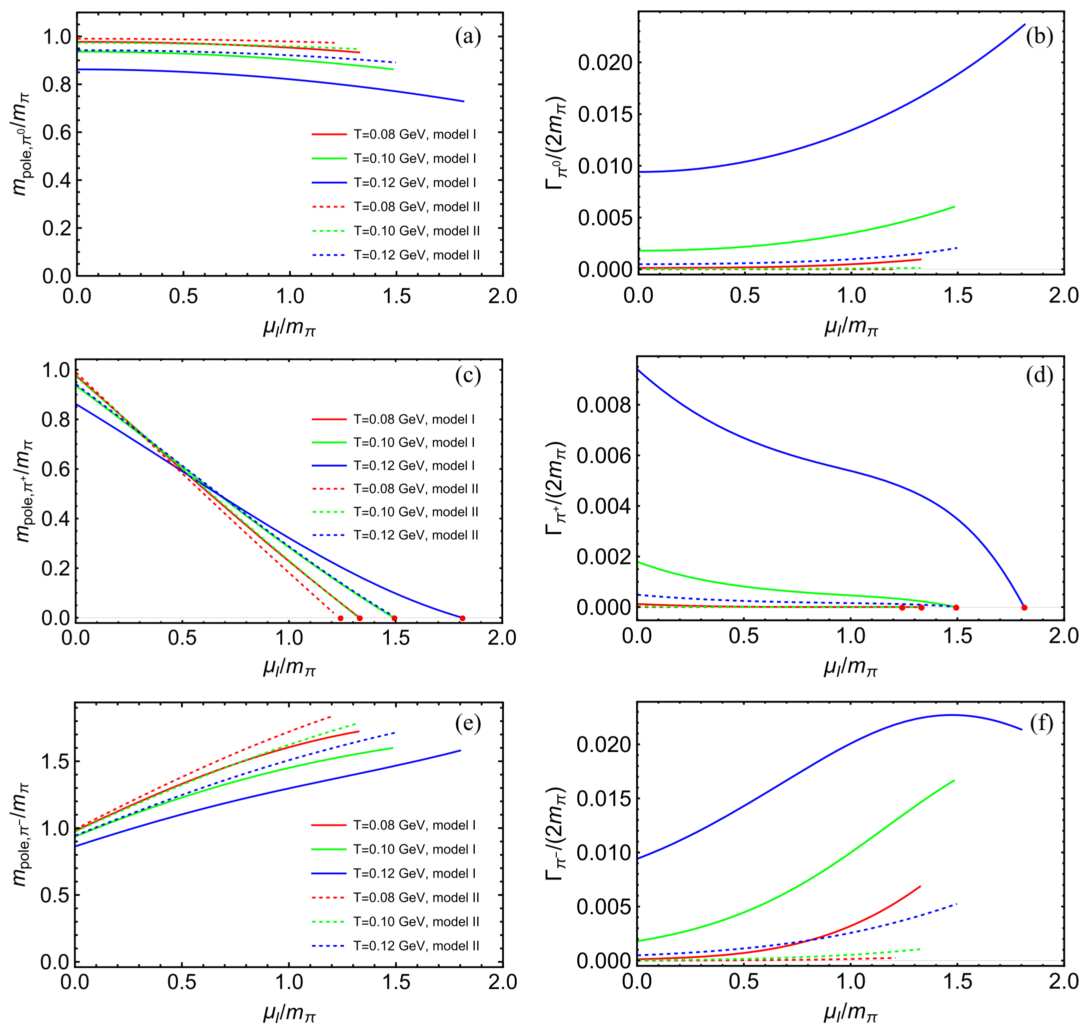

FIG. 7. Pole masses and thermal widths as functions of μ_I for (a),(b) π^0; (c),(d) π^+ and (e),(f) π^-. The red, green and blue lines stand for results at $T = 0.08, 0.10, 0.12$ GeV, respectively. The solid and dashed lines represent results in model I and II, respectively. m_{pole,π^+} and Γ_{π^+} vanish at $\mu_I/m_\pi = 1.32$, 1.49 and 1.82, respectively, in model I, and at $\mu_I/m_\pi = 1.24$, 1.31 and 1.49, respectively, in model II, as shown by the red dots.

same trend that m_{pole,π^0} and Γ_{π^0} vary monotonously with the increasing of μ_I. We find that isospin chemical potential μ_I has little impact on m_{pole,π^0} and Γ_{π^0} at low temperature, which is consistent with the analysis in Ref. [67]. This result may be reasonable since π^0 has no isospin charge and is almost independent on μ_I. The slight influence of isospin on π^0 mainly comes from the gravity background metric [See Eq. (9) and (12)].

As for π^+, the numerical results are shown in Figs. 7(c) and (d). We find that m_{pole,π^+} decreases almost linearly to zero with the increasing of μ_I. At the same time, the thermal width Γ_{π^+} also decreases to zero with the increasing of μ_I. In model I, both m_{pole,π^+} and Γ_{π^+} vanish when μ_I reaches $\mu_I^c = 0.184$ GeV with the fixed temperature $T = 0.08$ GeV. This implies the instability of the system and the emergence of pion superfluid phase transition. As the matter of fact, the points at which π^+ becomes a massless boson are exactly on the boundary between the pion condensed phase and the normal phase. In addition, we have the critical isospin chemical potential as

$$\begin{aligned} T/(\mathrm{GeV}) &= 0.08 \quad 0.10 \quad \text{and} \quad 0.12, \\ \text{Model I}: \mu_I^c/m_\pi &= 1.32 \quad 1.49 \quad \text{and} \quad 1.82, \\ \text{Model II}: \mu_I^c/m_\pi &= 1.24 \quad 1.31 \quad \text{and} \quad 1.49. \end{aligned}$$

Above μ_I^c, the $\mathrm{U}_I(1)$ symmetry, which is a subgroup of isospin $\mathrm{SU}(2)_I$, is broken and leads to the massless Goldstone boson $m_{\mathrm{pole},\pi^+} = 0$. This result is consistent with the NJL model [30]. However, since we do not take back reaction of the pion condensate into account, the study of the masses at $\mu_I > \mu_I^c$ will be left for our future work.

The numerical results for π^- are shown in Figs. 7(e) and (f). We find that m_{pole,π^-} increases monotonously with the increasing of μ_I at a fixed temperature. The thermal width Γ_{π^-} also increases monotonously with the increasing of μ_I in both models at low temperature. However, at high

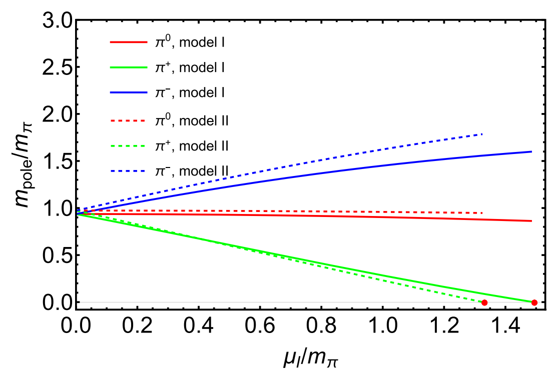

FIG. 8. Pole masses as functions of μ_I for the three modes π^0, π^+, π^- at $T = 0.10$ GeV in model I (represented by solid lines) and model II (represented by dashed lines). m_{pole} vanishes at $\mu_I^c = 1.49 m_\pi$ for model I and 1.32 m_π for model II, as shown by the red dots.

temperature, such as $T = 0.12$ GeV, the thermal width first increases and then decreases with the increasing of μ_I in model II.

Finally, we show the isospin chemical potential dependence of pole masses for the three modes together in Fig. 8 at fixed temperature $T = 0.10$ GeV. The qualitative behaviors are the same in both models. As a result of the explicit $\mathrm{SU_I}(2)$ symmetry breaking, the pole masses split at finite isospin chemical potential. It can be seen that m_{pole,π^+} vanishes at the critical isospin chemical potential μ_I^c, and m_{pole,π^0} almost keeps invariant, while m_{pole,π^-} increases with the increasing of μ_I. These results are consistent with the study in the hard-wall model [74], the NJL model [31] and our previous study by the spectral functions method [67].

IV. CONCLUSION

In this work, we investigate the temperature and isospin chemical potential dependence of the pion quasiparticle masses (screening mass, pole mass and thermal width) in the chiral symmetry breaking phase ($T < T_{cp}$) and normal phase ($\mu_I < m_\pi$) in the soft-wall AdS/QCD models. Furthermore, we also investigate the relation between the pion mass spectra and the pion superfluid phase transition. A comparative study on the two kinds of soft-wall models are shown. Both models provide consistent conclusions, which qualitatively reveals some common behaviors shared by the soft-wall AdS/QCD models.

On the one hand, we study the temperature dependence of the screening masses at fixed isospin chemical potentials. The results show that m_{scr,π^0} and $m_{\mathrm{scr},\pi^\pm}$ will split at finite μ_I, but $m_{\mathrm{scr},\pi^\pm}$ are degenerate in the normal phase. In this case, the screening masses of charged pions are lower than the neutral one at the same temperature. Both m_{scr,π^0} and $m_{\mathrm{scr},\pi^\pm}$ increase monotonously with the increasing of the temperature, and the difference between them decreases when T gets close to T_{cp}. Since π^0 carries no isospin charge, μ_I has little impact on m_{scr,π^0} which keeps unchanged with the increasing of μ_I. However, $m_{\mathrm{scr},\pi^\pm}$ decrease with the increased μ_I, and vanish at the critical isospin chemical potential μ_I^c, which implies the emergence of the pion superfluid phase transition. On the boundary between the normal phase and the pion superfluid phase, the $\mathrm{U}_I(1)$ symmetry is spontaneously broken, which leads to the appearance of the massless Goldstone boson π^+.

On the other hand, we also investigate the pole masses and thermal widths at finite temperature and isospin chemical potential, which are extracted from the corresponding QNMs. The results suggest that the pole masses and thermal widths of π^0, π^+, π^- will split at finite μ_I. We find that m_{pole,π^0} depends very weakly on μ_I, since it carries no isospin charge. However, m_{pole,π^+} decreases almost linearly with the increasing of μ_I and vanishes at the critical chemical potential μ_I^c, where π^+ becomes a massless Goldstone boson and pion superfluid phase transition take places. At low temperature region, m_{pole,π^-} increases almost linearly with the increasing of μ_I. However, at high temperature region, m_{pole,π^-} first increases and then decreases with the rise of μ_I. As for the temperature effect, both m_{pole,π^0} and m_{pole,π^-} decrease monotonously with the increasing of T. As for π^+, when μ_I is small, m_{pole,π^+} also decreases monotonously with the increasing of T. However, when μ_I gets larger, m_{pole,π^+} first increases to a certain maximum and then decreases with the rise of T. The thermal widths of the three modes increase with temperature. In this work, however, we do not consider the pion masses in the high-temperature phase above T_{cp} as well as in the pion superfluid phase, which will be left for future work.

ACKNOWLEDGMENTS

X. C. is supported by the National Natural Science Foundation of China under Grants No. 12275108, No. 12305142 and the Fundamental Research Funds for the Central Universities under Grant No. 21622324. H. L. is supported by the National Natural Science Foundation of China under Grant No. 11405074. D. L. is supported by the National Natural Science Foundation of China under Grants No. 12275108, No. 12235016, No. 11805084.

APPENDIX: COMPARISON WITH SPECTRAL FUNCTION METHOD

The pole mass results of model I, extracted from the QNMs, are almost in agreement with Ref. [67], in which model I is adopted, at low temperature. As shown in Fig. 9, we compare the isospin chemical potential dependence of pions obtained through QNM in this work with those of Ref. [67] at $T = 0.06$ GeV. The solid lines represent the pole masses of pions from QNMs. The dashed lines represent the pole masses of pions from spectral functions, taken from Ref. [67]. The results obtained by these two methods are in good agreement. However, one can see that there is a slight difference in the results obtained by these two methods. When extracting the pole masses from the pole of the spectral functions, due to the extraction and the availability of the Breit-Winger formula [68], slight differences arise and increase with the increasing temperature.

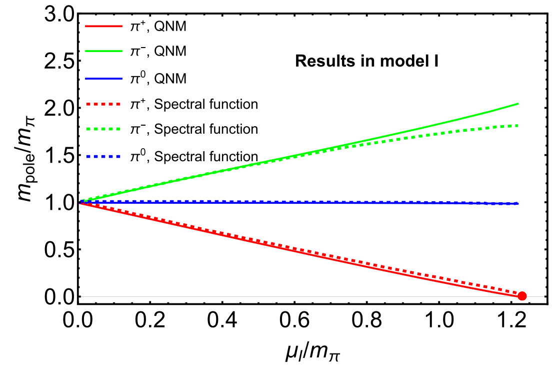

FIG. 9. Pole masses as functions of μ_I for π^0, π^+ and π^- at $T = 0.06$ GeV in model I. The solid lines represent results from QNMs. The dashed lines represent results from spectral functions [67]. The critical isospin chemical potential is $\mu_I^c \approx 0.170$ GeV.

[1] E. Shuryak, Strongly coupled quark-gluon plasma in heavy ion collisions, Rev. Mod. Phys. **89**, 035001 (2017).
[2] D. H. Rischke, The quark gluon plasma in equilibrium, Prog. Part. Nucl. Phys. **52**, 197 (2004).
[3] K. Fukushima and T. Hatsuda, The phase diagram of dense QCD, Rep. Prog. Phys. **74**, 014001 (2011).
[4] M. Huang and P. Zhuang, QCD matter and phase transitions under extreme conditions, Symmetry **15**, 541 (2023).
[5] A. Andronic, P. Braun-Munzinger, and J. Stachel, Thermal hadron production in relativistic nuclear collisions: The hadron mass spectrum, the horn, and the QCD phase transition, Phys. Lett. B **673**, 142 (2009); **678**, 516(E) (2009).
[6] M. Ishii, H. Kouno, and M. Yahiro, Model prediction for temperature dependence of meson pole masses from lattice QCD results on meson screening masses, Phys. Rev. D **95**, 114022 (2017).
[7] W. Florkowski, Description of hot compressed hadronic matter based on an effective chiral Lagrangian, Acta Phys. Pol. B **28**, 2079 (1997).
[8] M. Cheng *et al.*, Meson screening masses from lattice QCD with two light and the strange quark, Eur. Phys. J. C **71**, 1564 (2011).
[9] E. V. Shuryak, Physics of the pion liquid, Phys. Rev. D **42**, 1764 (1990).
[10] R. D. Pisarski and M. Tytgat, Propagation of cool pions, Phys. Rev. D **54**, R2989 (1996).
[11] X. Cao, M. Baggioli, H. Liu, and D. Li, Pion dynamics in a soft-wall AdS-QCD model, J. High Energy Phys. 12 (2022) 113.
[12] A. Ayala, C. A. Dominguez, M. Loewe, and Y. Zhang, Rho-meson resonance broadening in QCD at finite temperature, Phys. Rev. D **86**, 114036 (2012).
[13] C. A. Dominguez, M. Loewe, J. C. Rojas, and Y. Zhang, (Pseudo)scalar charmonium in finite temperature QCD, Phys. Rev. D **83**, 034033 (2011).
[14] C. A. Dominguez, M. Loewe, and Y. Zhang, Bottonium in QCD at finite temperature, Phys. Rev. D **88**, 054015 (2013).

[15] A. B. Migdal, Stability of vacuum and limiting fields, Zh. Eksp. Teor. Fiz. **61**, 2209 (1971).
[16] J. B. Kogut and D. K. Sinclair, Lattice QCD at finite isospin density at zero and finite temperature, Phys. Rev. D **66**, 034505 (2002).
[17] J. B. Kogut and D. K. Sinclair, The finite temperature transition for 2-flavor lattice QCD at finite isospin density, Phys. Rev. D **70**, 094501 (2004).
[18] C. Mu and P. Zhuang, Pion superfluidity beyond mean field approximation in Nambu-Jona-Lasinio model, Phys. Rev. D **79**, 094006 (2009).
[19] B. B. Brandt, A. Francis, H. B. Meyer, and D. Robaina, Chiral dynamics in the low-temperature phase of QCD, Phys. Rev. D **90**, 054509 (2014).
[20] B. B. Brandt, A. Francis, H. B. Meyer, and D. Robaina, Pion quasiparticle in the low-temperature phase of QCD, Phys. Rev. D **92**, 094510 (2015).
[21] Z. Fodor and S. D. Katz, A new method to study lattice QCD at finite temperature and chemical potential, Phys. Lett. B **534**, 87 (2002).
[22] D. T. Son and M. A. Stephanov, Pion propagation near the QCD chiral phase transition, Phys. Rev. Lett. **88**, 202302 (2002).
[23] D. T. Son and M. A. Stephanov, Real time pion propagation in finite temperature QCD, Phys. Rev. D **66**, 076011 (2002).
[24] R.-A. Tripolt, N. Strodthoff, L. von Smekal, and J. Wambach, Spectral functions for the quark-meson model phase diagram from the functional renormalization group, Phys. Rev. D **89**, 034010 (2014).
[25] Z. Wang and P. Zhuang, Meson spectral functions at finite temperature and isospin density with the functional renormalization group, Phys. Rev. D **96**, 014006 (2017).
[26] C. S. Fischer, QCD at finite temperature and chemical potential from Dyson–Schwinger equations, Prog. Part. Nucl. Phys. **105**, 1 (2019).
[27] F. Gao and M. Ding, Thermal properties of π and ρ meson, Eur. Phys. J. C **80**, 1171 (2020).
[28] D. Ebert, Y. L. Kalinovsky, and M. K. Volkov, Mesons at finite temperature in the NJL model with gluon condensate, Phys. Lett. B **301**, 231 (1993).
[29] L.-y. He, M. Jin, and P.-f. Zhuang, Pion superfluidity and meson properties at finite isospin density, Phys. Rev. D **71**, 116001 (2005).
[30] Y. Jiang, K. Ren, T. Xia, and P. Zhuang, Meson screening mass in a strongly coupled pion superfluid, Eur. Phys. J. C **71**, 1822 (2011).
[31] T. Xia, L. He, and P. Zhuang, Three-flavor Nambu–Jona-Lasinio model at finite isospin chemical potential, Phys. Rev. D **88**, 056013 (2013).
[32] J. Chao, M. Huang, and A. Radzhabov, Charged pion condensation in anti-parallel electromagnetic fields and nonzero isospin density, Chin. Phys. C **44**, 034105 (2020).
[33] H. Liu, X. Wang, L. Yu, and M. Huang, Neutral and charged scalar mesons, pseudoscalar mesons, and diquarks in magnetic fields, Phys. Rev. D **97**, 076008 (2018).
[34] K. Xu, J. Chao, and M. Huang, Effect of the anomalous magnetic moment of quarks on magnetized QCD matter and meson spectra, Phys. Rev. D **103**, 076015 (2021).
[35] B.-k. Sheng, X. Wang, and L. Yu, Impacts of inverse magnetic catalysis on screening masses of neutral pions and sigma mesons in hot and magnetized quark matter, Phys. Rev. D **105**, 034003 (2022).
[36] J. M. Maldacena, The large N limit of superconformal field theories and supergravity, Adv. Theor. Math. Phys. **2**, 231 (1998).
[37] S. S. Gubser, I. R. Klebanov, and A. M. Polyakov, Gauge theory correlators from noncritical string theory, Phys. Lett. B **428**, 105 (1998).
[38] E. Witten, Anti-de Sitter space and holography, Adv. Theor. Math. Phys. **2**, 253 (1998).
[39] J. Casalderrey-Solana, H. Liu, D. Mateos, K. Rajagopal, and U. A. Wiedemann, *Gauge/String Duality, Hot QCD and Heavy Ion Collisions* (Cambridge University Press, Cambridge, England, 2014).
[40] J. Erlich, E. Katz, D. T. Son, and M. A. Stephanov, QCD and a holographic model of hadrons, Phys. Rev. Lett. **95**, 261602 (2005).
[41] A. Karch, E. Katz, D. T. Son, and M. A. Stephanov, Linear confinement and AdS/QCD, Phys. Rev. D **74**, 015005 (2006).
[42] S. J. Brodsky, G. F. de Teramond, H. G. Dosch, and J. Erlich, Light-front holographic QCD and emerging confinement, Phys. Rep. **584**, 1 (2015).
[43] S. S. Gubser and A. Nellore, Mimicking the QCD equation of state with a dual black hole, Phys. Rev. D **78**, 086007 (2008).
[44] S. S. Gubser, A. Nellore, S. S. Pufu, and F. D. Rocha, Thermodynamics and bulk viscosity of approximate black hole duals to finite temperature quantum chromodynamics, Phys. Rev. Lett. **101**, 131601 (2008).
[45] O. DeWolfe, S. S. Gubser, and C. Rosen, A holographic critical point, Phys. Rev. D **83**, 086005 (2011).
[46] U. Gursoy and E. Kiritsis, Exploring improved holographic theories for QCD: Part I, J. High Energy Phys. 02 (2008) 032.
[47] U. Gursoy, E. Kiritsis, and F. Nitti, Exploring improved holographic theories for QCD: Part II, J. High Energy Phys. 02 (2008) 019.
[48] A. Cherman, T. D. Cohen, and E. S. Werbos, The chiral condensate in holographic models of QCD, Phys. Rev. C **79**, 045203 (2009).
[49] T. Gherghetta, J. I. Kapusta, and T. M. Kelley, Chiral symmetry breaking in the soft-wall AdS/QCD model, Phys. Rev. D **79**, 076003 (2009).
[50] D. Li, M. Huang, and Q.-S. Yan, A dynamical soft-wall holographic QCD model for chiral symmetry breaking and linear confinement, Eur. Phys. J. C **73**, 2615 (2013).
[51] P. Colangelo, F. Giannuzzi, S. Nicotri, and V. Tangorra, Temperature and quark density effects on the chiral condensate: An AdS/QCD study, Eur. Phys. J. C **72**, 2096 (2012).
[52] D. Li and M. Huang, Chiral phase transition of QCD with $N_f = 2 + 1$ flavors from holography, J. High Energy Phys. 02 (2017) 042.
[53] K. Chelabi, Z. Fang, M. Huang, D. Li, and Y.-L. Wu, Chiral phase transition in the soft-wall model of AdS/QCD, J. High Energy Phys. 04 (2016) 036.
[54] K. Chelabi, Z. Fang, M. Huang, D. Li, and Y.-L. Wu, Realization of chiral symmetry breaking and restoration in holographic QCD, Phys. Rev. D **93**, 101901 (2016).

[55] Z. Fang, Y.-L. Wu, and L. Zhang, Chiral phase transition and meson spectrum in improved soft-wall AdS/QCD, Phys. Lett. B **762**, 86 (2016).

[56] J. Chen, S. He, M. Huang, and D. Li, Critical exponents of finite temperature chiral phase transition in soft-wall AdS/QCD models, J. High Energy Phys. 01 (2019) 165.

[57] A. Ballon-Bayona and L. A. H. Mamani, Nonlinear realization of chiral symmetry breaking in holographic soft wall models, Phys. Rev. D **102**, 026013 (2020).

[58] A. Ballon-Bayona, L. A. H. Mamani, and D. M. Rodrigues, Spontaneous chiral symmetry breaking in holographic soft wall models, Phys. Rev. D **104**, 126029 (2021).

[59] Y. Chen and M. Huang, Holographic QCD model for Nf = 4, Phys. Rev. D **105**, 026021 (2022).

[60] P. Colangelo, F. De Fazio, F. Giannuzzi, F. Jugeau, and S. Nicotri, Light scalar mesons in the soft-wall model of AdS/QCD, Phys. Rev. D **78**, 055009 (2008).

[61] Y.-Q. Sui, Y.-L. Wu, Z.-F. Xie, and Y.-B. Yang, Prediction for the mass spectra of resonance mesons in the soft-wall AdS/QCD with a modified 5D metric, Phys. Rev. D **81**, 014024 (2010).

[62] T. M. Kelley, S. P. Bartz, and J. I. Kapusta, Pseudoscalar mass spectrum in a soft-wall model of AdS/QCD, Phys. Rev. D **83**, 016002 (2011).

[63] D. Li and M. Huang, Dynamical holographic QCD model for glueball and light meson spectra, J. High Energy Phys. 11 (2013) 088.

[64] E. Folco Capossoli and H. Boschi-Filho, Glueball spectra and Regge trajectories from a modified holographic softwall model, Phys. Lett. B **753**, 419 (2016).

[65] D. Dudal, D. R. Granado, and T. G. Mertens, No inverse magnetic catalysis in the QCD hard and soft wall models, Phys. Rev. D **93**, 125004 (2016).

[66] E. Folco Capossoli, M. A. Martín Contreras, D. Li, A. Vega, and H. Boschi-Filho, Hadronic spectra from deformed AdS backgrounds, Chin. Phys. C **44**, 064104 (2020).

[67] X. Cao, H. Liu, and D. Li, Pion quasiparticles and QCD phase transitions at finite temperature and isospin density from holography, Phys. Rev. D **102**, 126014 (2020).

[68] X. Cao, S. Qiu, H. Liu, and D. Li, Thermal properties of light mesons from holography, J. High Energy Phys. 08 (2021) 005.

[69] X. Chen, D. Li, D. Hou, and M. Huang, Quarkyonic phase from quenched dynamical holographic QCD model, J. High Energy Phys. 03 (2020) 073.

[70] Y.-Q. Zhao and D. Hou, Vector meson spectral function in a dynamical AdS/QCD model, Eur. Phys. J. C **82**, 1102 (2022).

[71] L. A. H. Mamani, D. Hou, and N. R. F. Braga, Melting of heavy vector mesons and quasinormal modes in a finite density plasma from holography, Phys. Rev. D **105**, 126020 (2022).

[72] X. Guo, J.-J. Jiang, X. Liu, D. Xiang, and X. Chen, Doubly-heavy tetraquark at finite temperature in a holographic model, arXiv:2306.06976.

[73] J. Erdmenger, N. Evans, W. Porod, and K. S. Rigatos, Gauge/gravity dual dynamics for the strongly coupled sector of composite Higgs models, J. High Energy Phys. 02 (2021) 058.

[74] B.-H. Lee, S. Mamedov, S. Nam, and C. Park, Holographic meson mass splitting in the nuclear matter, J. High Energy Phys. 08 (2013) 045.

[75] H. Nishihara and M. Harada, Enhancement of chiral symmetry breaking from the pion condensation at finite isospin chemical potential in a holographic QCD model, Phys. Rev. D **89**, 076001 (2014).

[76] H. Nishihara and M. Harada, Equation of state in the pion condensation phase in asymmetric nuclear matter using a holographic QCD model, Phys. Rev. D **90**, 115027 (2014).

[77] S. Mamedov, Meson effective mass in the isospin medium in hard-wall AdS/QCD model, Eur. Phys. J. C **76**, 83 (2016).

[78] N. Nasibova, Isospin symmetry of ω meson in the soft-wall model of holographic QCD at finite temperature, arXiv:2302.09889.

[79] M. Lv, D. Li, and S. He, Pion condensation in a soft-wall AdS/QCD model, J. High Energy Phys. 11 (2019) 026.

[80] X. Cao, H. Liu, D. Li, and G. Ou, QCD phase diagram at finite isospin chemical potential and temperature in an IR-improved soft-wall AdS/QCD model, Chin. Phys. C **44**, 083106 (2020).

[81] D. Teaney, Finite temperature spectral densities of momentum and R-charge correlators in $N = 4$ Yang Mills theory, Phys. Rev. D **74**, 045025 (2006).

[82] P. Kovtun and A. Starinets, Thermal spectral functions of strongly coupled $N = 4$ supersymmetric Yang-Mills theory, Phys. Rev. Lett. **96**, 131601 (2006).

[83] P. Colangelo, F. Giannuzzi, and S. Nicotri, Holographic approach to finite temperature QCD: The case of scalar glueballs and scalar mesons, Phys. Rev. D **80**, 094019 (2009).

[84] P. Colangelo, F. Giannuzzi, and S. Nicotri, In-medium hadronic spectral functions through the soft-wall holographic model of QCD, J. High Energy Phys. 05 (2012) 076.

[85] P. Lowdon and O. Philipsen, Pion spectral properties above the chiral crossover of QCD, J. High Energy Phys. 10 (2022) 161.

[86] P. K. Kovtun and A. O. Starinets, Quasinormal modes and holography, Phys. Rev. D **72**, 086009 (2005).

[87] A. S. Miranda, C. A. Ballon Bayona, H. Boschi-Filho, and N. R. F. Braga, Black-hole quasinormal modes and scalar glueballs in a finite-temperature AdS/QCD model, J. High Energy Phys. 11 (2009) 119.

[88] R. Chen, D. Li, K. Bitaghsir Fadafan, and M. Huang, Hadron spectra and pion form factor in dynamical holographic QCD model with anomalous 5D mass of scalar field, Chin. Phys. C **47**, 063106 (2023).

[89] R. L. Workman *et al.* (Particle Data Group), Review of particle physics, Prog. Theor. Exp. Phys. **2022**, 083C01 (2022).

[90] J. P. Boyd, *Chebyshev and Fourier Spectral Methods* (Dover Publications, New York, 2001).

[91] D. T. Son and A. O. Starinets, Minkowski space correlators in AdS/CFT correspondence: Recipe and applications, J. High Energy Phys. 09 (2002) 042.